

Superfluid flow and vortex nucleation in room temperature, nonlocal photon fluids

David Vocke¹, Kali Wilson¹, Francesco Marino², Iacopo

Carusotto³, Brian P. Anderson⁴, Patrik Öhberg¹, Daniele Faccio^{1*}

¹*Institute of Photonics and Quantum Sciences, Heriot-Watt University, Edinburgh EH14 4AS, UK*

²*Dipartimento di Fisica, Università di Firenze, Sezione di Firenze INFN,*

Via Sansone 1, I-50019 Sesto Fiorentino (FI), Italy

³*INO-CNR BEC Center and Dipartimento di Fisica, Università di Trento, I-38123 Povo, Italy and*

⁴*College of Optical Sciences, University of Arizona, Tucson, AZ, USA*

Superfluidity is a remarkable manifestation of quantum many-body effects at the macroscopic scale. Various features of superfluidity in liquid He and Bose-Einstein condensates remain challenging to study, limited by the complexity of the experiments or difficulty in measuring *in situ* all parameters of the wave function. There is therefore a continuous search for alternative superfluids to address these challenges. We demonstrate superfluid behaviour in a room-temperature system that relies on photons rather than atoms for the supporting fluid medium. The repulsive photon-photon interaction is mediated by a thermal optical nonlinearity and is inherently nonlocal. We experimentally observe the nucleation of quantised vortices from an extended physical obstacle and the nonlocal nature of the fluid is shown to deform the vortex geometry. Our results show that photon fluids provide a valid alternative to other superfluids with applications from the study of nonlinear wave turbulence and analogue gravity to artificial gauge fields.

Over the past decade, theoretical and experimental studies of photon fluids have opened up new ways of realising many-body systems. In the most general sense, a photon fluid is a collection of photons, *i.e.*, a laser beam propagating through a defocusing nonlinear medium such that the photons act as a gas of weakly interacting particles [1–4]. As in atomic many-body systems, the collective photon behaviour can be described by a Gross-Pitaevskii equation, where the electric field plays the role of the order parameter, a macroscopic wave function with a clear resemblance to dilute-gas Bose-Einstein condensates (BECs) and superfluid helium [5, 6]. The nucleation of quantised vortices is a hallmark of such superfluids, with vortices appearing as topological defects once the superfluid flow reaches a critical velocity and are characterised by a quantised circulation. Extending such studies of vortices to photon fluids would establish photon fluids as a new platform for probing general microscopic aspects of the breakdown of superfluidity, and vortex-vortex or vortex-surface interactions. However, evidence of similar processes of vortex nucleation in the wake of a photon fluid moving past an immersed obstacle has not been previously demonstrated.

Here we present experimental evidence of superfluid behaviour in nonlocal photon fluids flowing past an extended obstacle. While wave scattering by the obstacle is suppressed at low flow speeds, at higher flow speeds we observe the formation of quantised vortices in the wake of the obstacle that are characterised by both quantised circulation around a phase singularity and a corresponding region of zero intensity. The experiments also show an unexpected deformation of the vortices, which exhibit elliptical cores. Numerical simulations highlight how the nonlocality leads to a distributed

interaction with the extended obstacle, which in turn contributes to the elliptical nature of the nucleated vortices.

We first briefly describe the characteristics of quantised vortices in superfluids. The physics of quantised vortices has been of great interest ever since their discovery in ⁴He [7–9] and later in BECs [10], and their inherent dynamics are intensively studied in quantum turbulence [11]. Unfortunately, due to the relatively short coherence length in ⁴He, the vortex core diameter is of the order of a few Ångströms and is hard to visualise by optical means, although progress has been made using hydrogen tracer particles [12]. In contrast, in BECs and photon fluids, the diluteness of the fluid leads to larger healing lengths, with vortex core diameters on the order of half a micron and tens of microns respectively, allowing for direct observation [13, 14]. Furthermore, in photon fluids, straightforward optical interferometry provides easy access to phase information and thus photon fluids could provide an accessible platform to study quantised vortex dynamics, where core position, circulation and winding number can be easily identified. Recent optical experiments have been directed at exciton-polariton fluids, *i.e.* strongly coupled exciton-polaritons in semiconductor microcavities that have shown superfluid characteristics, such as the frictionless flow around an obstacle [15] and shedding of solitons [16] and quantised vortices [17, 18]. Differently from these driven-dissipative systems with local nonlinearity, signatures of superfluid behaviour in the dispersion relation have also been observed for room-temperature, nonlocal photon fluids in a propagating geometry [19]. Heating induced by a laser beam leads to a decrease in the refractive index of the medium and a consequent defocusing effect, *i.e.*, a repulsive photon-photon interaction. For a monochromatic beam,

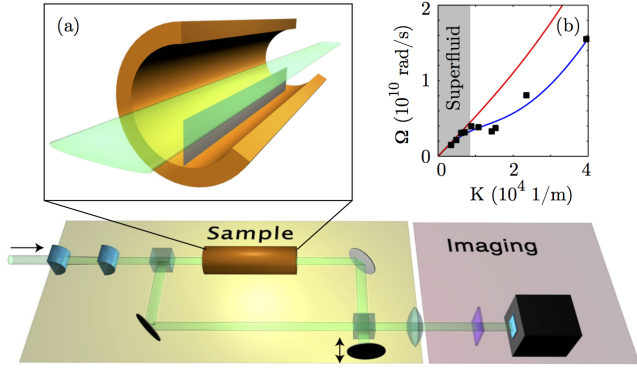


FIG. 1. (a) Experimental setup - A 532-nm laser beam with an elliptical spatial beam profile is launched into a sample filled with a methanol/graphene solution. A knife blade is mounted inside the sample and slightly tilted with respect to the propagation direction at an angle θ that determines the flow of the photon fluid [inset (a)]. Inset (b) shows the measured nonlocal dispersion relation of the photon fluid for beam diameters of 1 cm and 260 μm [19]. Solid red line - Bogoliubov dispersion relation, Eq. (4) with a local nonlinearity $\Delta n = 7.6 \times 10^{-6}$. Solid blue line - nonlocal dispersion relation with $\sigma_L = 110 \mu\text{m}$ and $\Delta n = 7.6 \times 10^{-6}$ and best fit to the experimental data (black circles).

the transverse beam profile acts as a two-dimensional fluid and is fully described by hydrodynamical equations, where the propagation direction maps into an effective time coordinate [2, 3]. Solitons and vortex solitons have been reported in these systems [14, 20], yet the nonlocal aspect of the interaction that is inherent to the physical origin of the photon-photon interactions has only attracted attention more recently [21], enabling studies of novel shock front and turbulence dynamics [22–24].

We now briefly recall the main features and equations describing photon fluids. Nonlinear propagation of a light beam in a defocusing medium can be described within the paraxial approximation [25] in terms of a nonlinear Schrödinger equation that is formally identical to the Gross-Pitaevskii equation for dilute boson gases with repulsive interaction [26],

$$\partial_z E = \frac{i}{2k} \nabla^2 E - i \frac{kn_2}{n_0} |E|^2 E, \quad (1)$$

where $k = 2\pi n_0/\lambda$ is the optical wavenumber, λ is the vacuum wavelength of the light, n_0 is the linear and n_2 the nonlinear refractive index, respectively. By considering the propagation direction z as time coordinate $t = zn_0/c$, where c is the speed of light in vacuum, and the electric field $E(\mathbf{r}, t) = \sqrt{\rho(\mathbf{r}, t)} \exp(i\phi(\mathbf{r}, t))$ as a function of fluid density ρ and phase ϕ , one arrives at a set of hydrodynamical equations that describes the laser

beam as a 2+1-dimensional quantum fluid of light [1, 4],

$$\partial_\tau \rho + \nabla(\rho \mathbf{v}) = 0 \quad (2)$$

$$\partial_\tau \psi + \frac{1}{2} v^2 + \frac{c^2 n_2}{n_0^3} \rho - \frac{c^2}{2k^2 n_0^2} \frac{\nabla^2 \sqrt{\rho}}{\sqrt{\rho}} = 0 \quad (3)$$

The gradient of the transverse beam phase determines the fluid flow velocity $\mathbf{v} = (c/kn_0)\nabla\phi = \nabla\psi$ and the speed of long-wavelength sonic waves is given by $c_s = \sqrt{c^2 |n_2| \rho / n_0^3}$.

Transverse wave perturbations propagating on an intense background beam obey the well known Bogoliubov dispersion relation [1, 4]. Considering nonlocal nonlinearities, an extension of the Bogoliubov theory leads to a modified form of the dispersion relation [27],

$$(\Omega - vK)^2 = \frac{c^2 |n_2| \rho}{n_0^3} \hat{R}(K, n_0 \Omega / c) K^2 + \frac{c^2}{4k^2 n_0^2} K^4, \quad (4)$$

relating frequency Ω and wavenumber K of phonon excitations. Here \hat{R} is the Fourier transform of the medium response function and can be modeled by a Lorentzian function, $\hat{R}(K) = [1 + \sigma_L^2 K^2]^{-1}$ [19], where the width of the response function σ_L defines the nonlocal length [27, 28]. For excitations with wavenumbers smaller than the inverse of the nonlocal length ($K < 1/\sigma_L$) the dispersion is a linear function in K ($\Omega \approx c_s K$). Using the parameters and the technique described in Ref. [19], we measured the $\Omega(K)$ spectrum of elementary excitations and indeed show that these follow the dispersion given by Eq. (4) with $\sigma_L = 110 \mu\text{m}$ and $\Delta n = |n_2| \rho = 7.6 \times 10^{-6}$ determined from the best fit to the experimental data [see Fig. 1(b)]. Hence there exists a critical velocity v_c for which a fluid with flow speed $v < v_c$ behaves as a superfluid and is not perturbed by small weak defects inserted in the flow. For local fluids, the critical velocity is determined by the speed of sound; as it is discussed in full detail in the appendix, the nonlocality can significantly reduce the critical velocity. For the experimental parameters, this reduction amounts to approximately a factor of two. Furthermore, in this work we consider an extended impenetrable obstacle such that the local flow speed can become supercritical in its vicinity, even if the asymptotic speed v_f far from the obstacle remains subcritical. In this case we would expect the flow to become non-laminar and thus generate excitations and topological defects, such as quantized vortices [29]. These effects, although well known in local media ($\hat{R} = 1$), have not been experimentally observed or studied in nonlocal media.

The experimental setup is shown in Fig. 1. We launch a highly elliptical CW laser beam with wavelength $\lambda = 532$ nm through a cylindrical cell with length $L = 18$ cm and diameter $D = 2$ cm, filled with a methanol/graphene solution as a thermal nonlinear medium. Methanol has a negative thermo-optic coefficient of $dn/dT = -4 \times 10^{-4}$ 1/K (providing the repulsive photon-photon interaction)

while nanometric graphene flakes are added in order to increase the absorption coefficient to $\alpha = 0.035 \text{ cm}^{-1}$ and ensure sufficient thermo-optic nonlinearity at the input intensities (of the order $4\text{-}7 \text{ W/cm}^2$) used in the experiments. The beam is loosely focused onto the sample by a set of cylindrical lenses with a minor axis diameter of either $900 \text{ }\mu\text{m}$ [Fig. 2(a)-(b)] or $300 \text{ }\mu\text{m}$ [Fig. 2(c)-(f)]. The sample is placed in one arm of a Mach-Zehnder interferometer. The other arm is used to probe the spatial phase profile of the output with a reference beam. To this end, a piezo-controlled delay stage is introduced in order to retrieve the full phase information by a phase-shifting interferometry technique [30]. Finally, the cell output is imaged with 4x magnification onto a CCD camera. As an obstacle, a knife blade is immersed in the sample along the beam path [see inset (a), Fig. 1] so that the beam propagation axis is at a slight angle θ with respect to the knife axis, thus introducing a relative transverse flow $v_f = (c/n_0) \sin \theta$, determined by the respective angle θ . Figures 2(a) and (b) show the normalised near-field intensity profile at the sample output $I(x, y, z = 18 \text{ cm})/I_0$ for the low ($I_0 = 0.2 \text{ W/cm}^2$, input intensity) and high nonlinearity regimes ($I_0 = 3.8 \text{ W/cm}^2$), respectively, with θ chosen to create a flow speed $v_f = 6 \times 10^5 \text{ m/s}$ along the positive x-axis. At low nonlinearity there is no superfluid flow, which is manifested by waves being scattered from the tip of the obstacle [seen as waves in the upper right-hand corner of Fig. 2(a)]. At high nonlinearity, where we expect superfluid flow, we estimate from the input parameters $\Delta n = 2.9 \times 10^{-5}$ [19] thus leading to a speed of sound of $c_s \sim 1.1 \times 10^6 \text{ m/s}$ that is significantly larger than the flow speed ($v_f/c_s \sim 0.5$) and excitations from the tip of the obstacle are partially suppressed [seen as a suppression of wave emission in the upper right-hand corner of Fig. 2(b)]. Note that the scattering of waves is indeed not fully suppressed due to the spatial decay of light intensity due to absorption, which causes a corresponding decay of the speed of sound, as well as due to the size of the obstacle that is much larger than the healing length ($\xi \sim 30\text{--}40 \mu\text{m}$), its rigidity that allows no penetration, and the sudden switch-on of its interaction with the photon fluid. Waves are thus also back-scattered from the obstacle and interfere with the incoming flow, explaining the structures seen in the lower part of the figure.

The breakdown of superfluidity leads to dissipation and drag forces on the obstacle and consequently, the nucleation of quantised vortices is expected to appear in the local interaction case [18, 31]. Figures 2(c)-(f) show experimental evidence in our *nonlocal* superfluid of the breakdown of the viscousless flow and the nucleation of quantised vortices that are considered to be hallmark evidence of superfluid behaviour. In these experiments we have chosen a higher transverse flow speed $v_f \sim 1.3 \times 10^6 \text{ m/s}$ and a minor-axis beam diameter of $300 \text{ }\mu\text{m}$. The measured intensity (fluid density) profiles

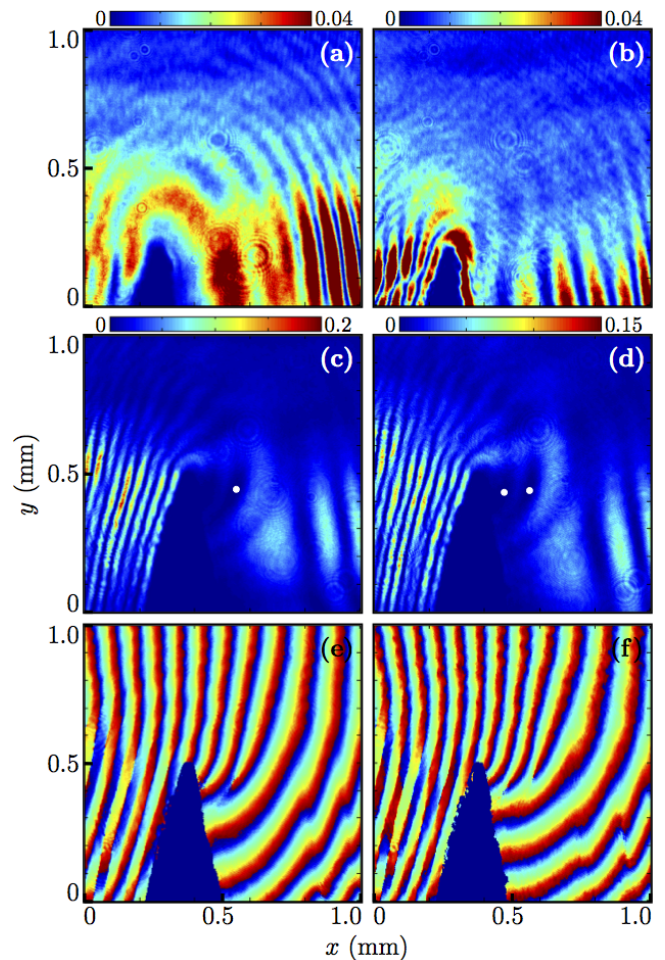


FIG. 2. Experimental measurements of the near-field beam profile at the sample output $I(x, y)/I_0$, normalised by input beam intensity I_0 . (a) and (b) $I(x, y)/I_0$ is capped at 0.04 to emphasize waves scattered from the obstacle into the upper right-hand region of each panel. (a) $v_f \sim 6 \times 10^5 \text{ m/s}$ and $I_0 = 0.2 \text{ W/cm}^2$ (linear propagation, i.e. non-superfluid regime). (b) $v_f \sim 6 \times 10^5 \text{ m/s}$ and $I_0 = 3.8 \text{ W/cm}^2$ (non-linear propagation, i.e. superfluid regime with $v_f/c_s \sim 0.5$). (c) and (d) $I(x, y)/I_0$ showing superfluid instability at higher flow speed, $v_f \sim 1.3 \times 10^6 \text{ m/s}$: (c) $I_0 = 4.0 \text{ W/cm}^2$ i.e. $\Delta n = 3.0 \times 10^{-5}$ and $v_f/c_s \sim 1.2$ and (d) $I_0 = 6.8 \text{ W/cm}^2$ i.e. $\Delta n = 5.2 \times 10^{-5}$ and $v_f/c_s \sim 0.9$. White circles indicate the position of the vortex singularities obtained from the corresponding phase diagrams shown in (e) and (f), respectively.

are shown in Figs. 2(c) and (d), for two different input intensities corresponding to two different sound speeds, i.e., $v_f/c_s \sim 1.2$ and $v_f/c_s \sim 0.9$, respectively. The intensity profiles show how the rigid obstacle creates a wake in the downstream region, but just as in an ordinary fluid, the light intensity is able to flow around the tip of the obstacle and fill in the shadowed region. A series of vortices (dark regions in the intensity profile, marked with white dots) are seen to nucleate from close to the tip. One vortex is observed for $v_f/c_s \sim 1.2$ and a second vortex is formed for higher excitation (i.e. sound) speeds,

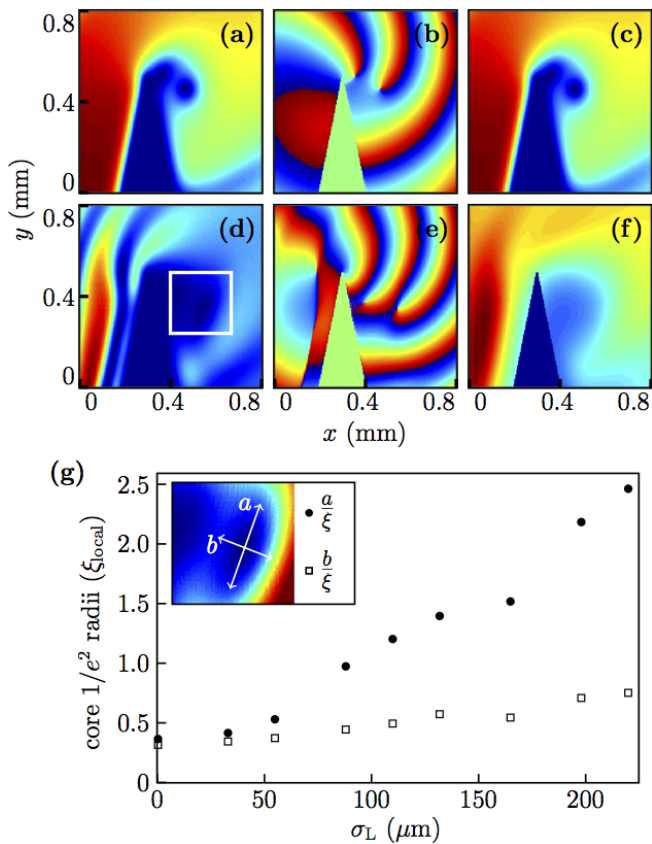


FIG. 3. Numerical results - (a) $I(x, y)/I_0$, (b) $\phi(x, y)$ and (c) $\Delta n(x, y)/\Delta n$, for a purely local superfluid after 20 cm of propagation, with $\sigma_L = 0 \mu\text{m}$, $v_f/c_s = 0.56$, $\Delta n = 1.2 \times 10^{-5}$, and $1/e^2$ beam radii $w_x = w_y = 1 \text{ mm}$. (d), (e) and (f) show the corresponding profiles for a nonlocal superfluid with $\sigma_L = 110 \mu\text{m}$, and $\Delta n = 2.4 \times 10^{-5}$. (g) Plot of vortex core $1/e^2$ radii, a and b , normalized to the healing length ξ , versus σ_L . The inset, corresponding to the white region in (d), shows a vortex core with labeled major axis a and minor axis b .

$v_f/c_s \sim 0.9$. This interpretation finds confirmation in the phase profiles shown in Figs. 2(e) and (f) where the drag on the obstacle is visualised by the bending of the phase pattern around the tip of the obstacle. The nucleation of vortices in the wake of the obstacle is evidenced by the clockwise circulating phase singularities. A notable feature is that the vortices do not appear to nucleate exactly at the tip of the obstacle and moreover, they have a clearly elliptical shape.

To further understand the vortex nucleation and the role of nonlocality in this process, we performed numerical simulations based on a split-step propagation of Eq. (1), including also linear absorption. The absorption and obstacle shape are chosen to match the experiment. However, we chose a circular Gaussian input beam (with 1-mm $1/e^2$ beam radius) in order to avoid the contribution of asymmetric defocusing related to beam asymmetry. Grid spacing is chosen such that $\Delta x = \Delta y = 3.9 \mu\text{m}$, well below the smallest expected values of the healing

length $\xi \sim 20 - 30 \mu\text{m}$. Nonlocality is described by the same Lorentzian function \hat{R} described above, with $K^2 = k_x^2 + k_y^2$. As in the experiment, we numerically find asymmetric vortex cores with radii larger than the local healing length that nucleate from a point on the downstream edge of the blade rather than off its tip. We interpret these observations as due in part to the nonlocality of the superfluid and further explore these nonlocal effects in the numerics, as shown in Fig. 3. Figures 3(a)-(c) show the normalised intensity $I(x, y)/I_0$, phase $\phi(x, y)$ and effective nonlinear potential energy $\Delta n(x, y)/\Delta n$ profiles, respectively, for a purely local superfluid with $\sigma_L = 0 \mu\text{m}$ after 20 cm of propagation. Figures 3(d)-(f) show the corresponding profiles for a nonlocal superfluid with $\sigma_L = 110 \mu\text{m}$. Videos showing the full evolution of the fluid and the vortex nucleation for both the symmetric beam shown in Fig. 3, and a highly elliptical beam are presented in the appendix. Although we have chosen specific parameter values for these results, we verified that vortex nucleation is still observed over a wide range of values for both σ and Δn that can vary by more than an order of magnitude, thus indicating that the observations and physical phenomena are generic features of these photon fluids. We first note that in the local fluid the vortex cores are nucleated at the tip of the knife blade as shown in Fig. 3(b), whereas in the nonlocal case Fig. 3(e) shows the vortex cores nucleating further down from the tip. The nucleation point moves downward as we increase σ_L and can be attributed to the fluid interacting with an extended surface along the knife-blade edge, rather than only the tip. In other words, the nonlocality smoothens the effective nonlinear potential energy term, as shown by the $\Delta n(x, y)$ profile in Fig. 3(f) so that the spatial extent of the knife blade felt by any point in the fluid increases as we increase the nonlocality. Given that the sharpness of a feature is determined by the balance between the diffraction (kinetic energy) and the nonlinear term (effective potential energy), the smearing of the nonlinear term results in the fluid no longer being able to support sharp features and effectively increases the healing length and the observed core radii.

In order to examine in more detail the effect of nonlocality on the ellipticity of the vortex cores, in Fig. 3(g) we plot the vortex core $1/e^2$ radii a, b (normalised to a local healing length $\xi = \lambda/\sqrt{4n_0|n_2|\rho}$ so as to account for any local variation in the fluid density associated with the output beam intensity) as a function of increasing nonlocality, σ_L . For each value of σ_L , the input power is chosen such that we observe one clearly defined vortex core, and flow speed is adjusted to maintain a constant $v_f/c_s = 0.56$. At $\sigma_L = 0 \mu\text{m}$ the vortex cores are circular [$a/\xi = b/\xi$, as seen also in Fig. 3(a)]. However, as we increase σ_L , we observe a continuous increase in the core aspect ratio, in keeping with the nonlocal smearing of the nonlinear potential along the obstacle edge as shown in

Fig. 3(f).

Summarising, we have provided evidence of nucleation of quantised vortices from an extended hard obstacle in a flowing photon fluid, thus providing hallmark evidence for superfluidity in a room-temperature system. The nonlocal nature of the photon fluid does not suppress superfluidity but rather deforms the nonlinear potential which is smeared across the extended obstacle surface and thus in turn influences the geometry of the nucleated vortex cores. Such nonlocal superfluids are of relevance in relation to recent proposals for studying horizon and Hawking-like emission in artificial spacetime geometries that mimic Lorentz-invariance based on the superfluid dispersion relation [2, 32–34], or for cases in which it is the nonlocality itself that is used to mimic long-range gravitational effects [35]. Photon fluids also provide an alternative testbed for nonlocal effects observed in dipolar BECs [36–39]. In closing, it is worth noting an interesting complementarity with respect to standard superfluids. In a material fluid like an atomic BEC or liquid He, one might argue that the nucleation of vortices is not particularly surprising. Yet the fact that the circulation of these vortices is quantised, indicating an underlying order parameter, is truly remarkable. Conversely, in a photon fluid the existence of an “order parameter”, i.e. a wave function that describes the optical beam as a whole, is rather trivial. Here, the remarkable aspect is the observation of a hydrodynamical mechanism for vortex nucleation when the light beam hits a physical obstacle. It is the co-presence of an effective order parameter and quantised vorticity that indicates the superfluid nature of the supporting medium, made of photons rather than atoms.

D.F. acknowledges financial support from the European Research Council under the European Unions Seventh Framework Programme (FP/20072013)/ERC GA 306559 and EPSRC (UK, Grant EP/J00443X/1). I. C. acknowledges financial support by the ERC through the QGBE grant, by the EU-FET Proactive grant AQuS, Project No. 640800, and by the Autonomous Province of Trento, partly through the SiQuoro project (“On Silicon Chip Quantum Optics for Quantum Computing and Secure Communications”).

APPENDIX

Here we provide further details on the effect of nonlocal interactions on the Landau critical velocity. The starting point of this discussion is the Bogoliubov dispersion of collective excitations in such a *nonlocal fluid* when this is at rest. After simple manipulation of eq.(4) of the Main Text, this can be written in the more usual form [40]:

$$\hbar\Omega(k) = \sqrt{\frac{\hbar^2 k^2}{2m} \left(\frac{\hbar^2 k^2}{2m} + \frac{2g\rho}{1 + k^2 \sigma_L^2} \right)} \quad (5)$$

that allows for transparent analytical manipulations and easier connection to the many-body literature. With respect to the usual case of a local fluid [41, 42], the nonlocality enters via the denominator of the interaction term that suppresses interactions at large k . For a propagating fluid of light, the frequency Ω corresponds to the wavevector k_z in the propagation direction expressed in temporal units, $\Omega = k_z c/n_0$, and k is the transverse wavevector (note the different convention from [43]).

In terms of the optical parameters of the optical medium,

$$m = \frac{\hbar n_0 k_0}{c} \quad (6)$$

is the effective mass of the photons, $\rho = |E|^2$ is the fluid density,

$$g = \frac{\hbar c k_0}{n_0^2} \chi^{(3)} \quad (7)$$

is the interaction constant, and the nonlocality is again modeled with a Lorentzian function of size σ_L . Here, n_0 is the background refractive index and $k_0 = 2\pi n_0/\lambda$ the free wavevector in the medium, and $\chi^{(3)}$ is the optical nonlinearity. The units of this latter are such that $\Delta n = \chi^{(3)}\rho$ is the nonlinear refractive index shift.

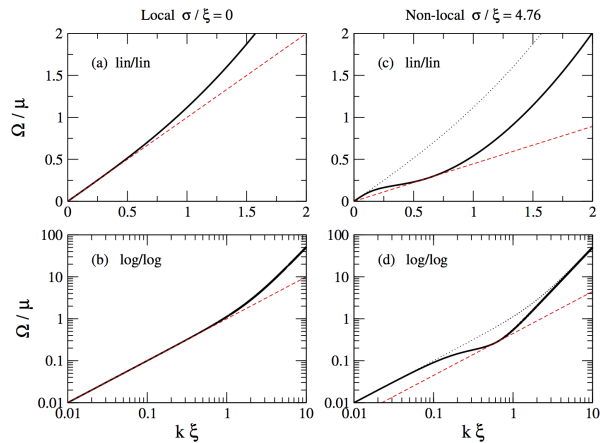


FIG. 4. Bogoliubov dispersion in a fluid at rest: the left (a,c) panels are for a local fluid $\sigma_L/\xi = 0$, the right (b,d) panels are for a nonlocal fluid with a value of $\sigma_L/\xi = 4.76$ inspired by the experiment. The dotted curve in the right panels repeats the local fluid dispersion for comparison. The red dashed line is the straight line $\Omega = v_c k$ corresponding to the critical speed v_c . The panels in the bottom row show the same curves in log-log scale.

Examples of such a Bogoliubov dispersion are shown in Fig.4 both in linear-linear and in log-log scales. The Landau critical velocity is defined as the minimum of the phase velocity $v_c = \min_k v_{\text{ph}}(k)$ where in our case

$$v_{\text{ph}}(k) = \frac{\Omega(k)}{k} = \left[\frac{\hbar^2 k^2}{4m^2} + \frac{g\rho/m}{1 + k^2 \sigma_L^2} \right]^{1/2}. \quad (8)$$

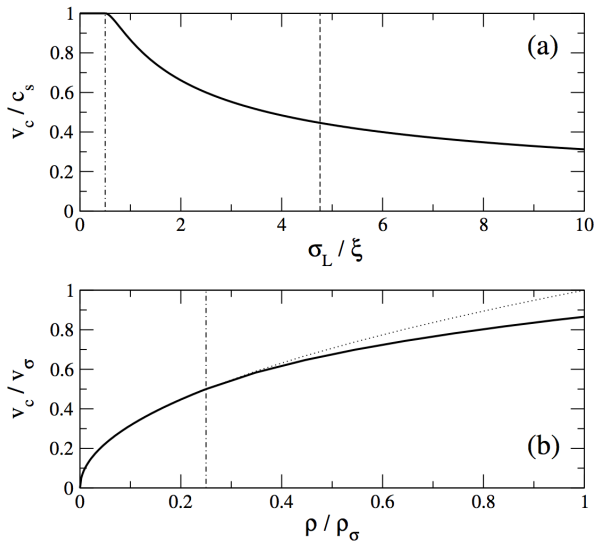


FIG. 5. Plots of the dependence of v_c on the nonlocal length σ_L [upper panel (a)] and on the density ρ [lower panel (b)]. In this latter, the density is normalized to $\rho_\sigma = \hbar^2/mg\sigma_L^2$ and the velocity to $v_\sigma = \hbar/m\sigma_L$. The vertical dot-dashed lines indicate the transition points between the two $\sigma_L \lesseqgtr \xi/2$ regimes. The vertical dashed line in the upper panel indicate the experimental conditions. The dotted line in the lower panel shows how $\sqrt{\rho}$ behaviour would extend to the whole domain.

Depending on the relative value of the nonlocality length σ_L and of the healing length

$$\xi = \sqrt{\frac{\hbar^2}{g\rho m}} = \sqrt{\frac{n_0}{\Delta n}} k_0^{-1}, \quad (9)$$

two regimes can be identified:

- For weak nonlocalities $\sigma_L < \xi/2$ [Fig.4(a,b)], the phase velocity $v(k)$ is a monotonically growing function of k , so the minimum is attained at $k = 0$. The critical Landau speed is then the speed of sound,

$$v_c = \lim_{k \rightarrow 0} \frac{\Omega(k)}{k} = \sqrt{\frac{g\rho}{m}} = \frac{c}{n_0} \sqrt{\frac{\Delta n}{n_0}} = c_s. \quad (10)$$

- For strong nonlocalities $\sigma_L > \xi/2$ [Fig.4(c,d)], the phase velocity $v(k)$ has a local minimum at

$$k_c = \sqrt{\frac{1}{\sigma_L} \left(\frac{2}{\xi} - \frac{1}{\sigma_L} \right)} \quad (11)$$

where it attains the smaller value

$$v_c = \sqrt{\frac{\hbar^2}{m^2\sigma_L} \left[\frac{1}{\xi} - \frac{1}{4\sigma_L} \right]} \quad (12)$$

Plots of the critical velocity v_L as a function of the nonlocality length and of the fluid density are shown in

the two panels of Fig.5. The former clearly shows that the critical velocity is equal to the sound velocity upto $\sigma_L = \xi/2$, then it quickly decays to zero according to the formulas:

$$v_c/c_s = 1 \quad \text{for } \sigma_L < \xi/2 \quad (13)$$

$$v_c/c_s = \sqrt{\frac{\xi}{\sigma_L} - \frac{\xi^2}{4\sigma_L^2}} \quad \text{for } \sigma_L > \xi/2. \quad (14)$$

The latter shows the usual $\sqrt{\rho}$ dependence at low ρ , which then transforms into a slower $\rho^{1/4}$ law at high ρ according to the formulas:

$$v_c = \sqrt{g\rho/m} \quad \text{for } \sigma_L < \xi/2 \quad (15)$$

$$v_c = \frac{\hbar}{m\sigma_L} \sqrt{\sqrt{\frac{\sigma_L^2 m g \rho}{\hbar^2}} - \frac{1}{4}} \quad \text{for } \sigma_L > \xi/2. \quad (16)$$

Note that the two regimes continuously connect at the transition point $\sigma_L = \xi/2$.

For the parameters of the experiment $\Delta n = 7.6 \times 10^{-6}$ with a background refractive index estimated around $n_0 \simeq 1.33$, one has $\sigma_L/\xi \approx 4.76$ which gives a factor ≈ 2 reduction of the critical velocity v_c below the speed of sound c_s .

* dev1@hw.ac.uk, d.faccio@hw.ac.uk

- [1] Carusotto, I. & Ciuti, C. Quantum fluids of light. *Rev. Mod. Phys.* **85**, 299–366 (2013).
- [2] Carusotto, I. Superfluid light in bulk nonlinear media. *Proc. R. So. A* **470**, 20140320–20140320 (2014).
- [3] Larré, P.-E. & Carusotto, I. Propagation of a quantum fluid of light in a cavityless nonlinear optical medium: General theory and response to quantum quenches. *Phys. Rev. A* **92**, 043802 (2015).
- [4] Chiao, R. & Boyce, J. Bogoliubov dispersion relation and the possibility of superfluidity for weakly interacting photons in a two-dimensional photon fluid. *Phys. Rev. A* **60**, 4114–4121 (1999).
- [5] Klaers, J., Schmitt, J., Vewinger, F. & Weitz, M. Bose-Einstein condensation of photons in an optical microcavity. *Nature* **468**, 545–548 (2010).
- [6] Balili, R., Hartwell, V., Snoke, D., Pfeiffer, L. & West, K. Bose-Einstein condensation of microcavity polaritons in a trap. *Science* **316**, 1007–10 (2007).
- [7] Onsager, L. Statistical hydrodynamics. *Il Nuovo Cimento* **6**, 279–287 (1949).
- [8] Feynman, R. P. Application of Quantum Mechanics to Liquid helium. *Prog. Low Temp. Phys.* **1**, 17–53 (1955).
- [9] Vinen, W. F. Mutual Friction in a Heat Current in Liquid Helium II. I. Experiments on Steady Heat Currents. *Proc. R. So. A* **240**, 114–127 (1957).
- [10] Matthews, M. R. *et al.* Vortices in a Bose-Einstein Condensate. *Phys. Rev. Lett.* **83**, 2498 (1999).
- [11] Tsubota, M. Quantum turbulence: from superfluid helium to atomic Bose-Einstein condensates. *Contemp. Phys.* **50**, 463–475 (2009).
- [12] Paoletti, M. S., Fisher, M. E., Sreenivasan, K. R. & Lathrop, D. P. Velocity Statistics Distinguish Quantum Turbulence from Classical Turbulence. *Phys. Rev. Lett.* **101**, 154501 (2008).

- [13] Wilson, K. E., Newman, Z. L., Lowney, J. D. & Anderson, B. P. *In situ* imaging of vortices in bose-einstein condensates. *Phys. Rev. A* **91**, 023621 (2015).
- [14] Swartzlander, G. & Law, C. Optical vortex solitons observed in Kerr nonlinear media. *Phys. Rev. Lett.* **69** (1992).
- [15] Amo, A. *et al.* Superfluidity of polaritons in semiconductor microcavities. *Nature Phys.* **5**, 805–810 (2009).
- [16] Amo, A. *et al.* Polariton superfluids reveal quantum hydrodynamic solitons. *Science* **332**, 1167–1170 (2011).
- [17] Sanvitto, D. *et al.* All-optical control of the quantum flow of a polariton condensate. *Nature Photon.* **5**, 610–614 (2011).
- [18] Nardin, G. *et al.* Hydrodynamic nucleation of quantized vortex pairs in a polariton quantum fluid. *Nature Phys.* **7**, 635–641 (2011).
- [19] Vocke, D. *et al.* Experimental characterization of nonlocal photon fluids. *Optica* **2**, 484 (2015).
- [20] Conti, C., Fratolocci, A., Peccianti, M., Ruocco, G. & Trillo, S. Observation of a Gradient Catastrophe Generating Solitons. *Phys. Rev. Lett.* **102**, 083902 (2009).
- [21] Ghofraniha, N. *et al.* Measurement of scaling laws for shock waves in thermal nonlocal media. *Opt. Lett.* **37**, 2325–2327 (2012).
- [22] Wan, W., Jia, S. & Fleischer, J. W. Dispersive superfluid-like shock waves in nonlinear optics. *Nature Phys.* **3**, 46–51 (2007).
- [23] Ghofraniha, N., Conti, C., Ruocco, G. & Trillo, S. Shocks in Nonlocal Media. *Phys. Rev. Lett.* **99**, 043903 (2007).
- [24] Xu, G. *et al.* From coherent shocklets to giant collective incoherent shock waves in nonlocal turbulent flows. *Nature Commun.* **6**, 8131 (2015).
- [25] Boyd, R. *Nonlinear Optics* (Academic Press, Burlington, 3rd edn., 2008).
- [26] Pethick, C. & Smith, H. *Bose-Einstein Condensation in Dilute Gases* (Cambridge University Press, Cambridge, 2nd edn., 2008).
- [27] Bar-Ad, S., Schilling, R. & Fleurov, V. Nonlocality and fluctuations near the optical analog of a sonic horizon. *Phys. Rev. A* **87**, 013802 (2013).
- [28] Minovich, A., Neshev, D. N., Dreischuh, A., Krolikowski, W. & Kivshar, Y. S. Experimental reconstruction of nonlocal response of thermal nonlinear optical media. *Opt. Lett.* **32**, 1599–601 (2007).
- [29] Winiecki, T., Jackson, B., McCann, J. F. & Adams, C. S. Vortex shedding and drag in dilute bose-einstein condensates. *J. Phys. B* **33**, 4069 (2000).
- [30] Kinnstaetter, K., Lohmann, A. W., Schwider, J. & Streibl, N. Accuracy of phase shifting interferometry. *Appl. Opt.* **27**, 5082–5089 (1988).
- [31] Inouye, S. *et al.* Observation of Vortex Phase Singularities in Bose-Einstein Condensates. *Phys. Rev. Lett.* **87**, 080402 (2001).
- [32] Marino, F. Acoustic black holes in a two-dimensional photon fluid. *Phys. Rev. A* **78**, 063804 (2008).
- [33] Fouxon, I., Farberovich, O. V., Bar-Ad, S. & Fleurov, V. Dynamics of fluctuations in an optical analogue of the Laval nozzle. *EPL (Europhys. Lett.)* **92**, 14002 (2010).
- [34] Fleurov, V. & Schilling, R. Regularization of fluctuations near the sonic horizon due to the quantum potential and its influence on Hawking radiation. *Phys. Rev. A* **85**, 045602 (2012).
- [35] R.Bekenstein, Schley, R., Mutzafi, M., Rotschild, C. & Segev, M. Optical simulations of gravitational effects in the Newton-Schrödinger system. *Nature Phys.* **11**, 1 (2015).
- [36] Strinati, M. C. & Conti, C. Bose-Einstein condensation of photons with nonlocal nonlinearity in a dye-doped graded-index microcavity. *Phys. Rev. A* **90**, 043853 (2014).
- [37] Lahaye, T., Menotti, C., Santos, L., Lewenstein, M. & Pfau, T. The physics of dipolar bosonic quantum gases. *Reports on Progress in Physics* **72**, 126401 (2009).
- [38] Wilson, R. M., Ronen, S., Bohn, J. L. & Pu, H. Manifestations of the Roton Mode in Dipolar Bose-Einstein Condensates. *Phys. Rev. Lett.* **100**, 245302 (2008).
- [39] Santos, L., Shlyapnikov, G. & Lewenstein, M. Roton-Maxon Spectrum and Stability of Trapped Dipolar Bose-Einstein Condensates. *Phys. Rev. Lett.* **90**, 250403 (2003).
- [40] Pomeau Y. and Rica S., Model of superflow with Rotons, *Phys. Rev. Lett.* **71**, 247 (1993).
- [41] Pitaevskii L.P. and Stringari S., *Bose-Einstein Condensation*, Clarendon Press Oxford (2003).
- [42] Carusotto I. and Ciuti C., Quantum Fluids of Light, *Rev. Mod. Phys.* **85**, 299 (2013).
- [43] Carusotto I., Superfluid light in bulk nonlinear media, *Proceedings of the Royal Society A: Mathematical, Physical and Engineering Sciences* **470**, 20140320 (2014).